Site-Directed Dichroism As a Method for Obtaining Rotational and Orientational Constraints for Oriented Polymers

Isaiah T. Arkin,[†,§,‡] **Kevin R. MacKenzie,**[‡] **and Axel T. Brünger***[,†,‡]

Contribution from the Howard Hughes Medical Institute and Department of Molecular Biophysics and Biochemistry, Yale University, New Haven, Connecticut 06520

Received December 10, 1996. Revised Manuscript Received May 15, 1997[⊗]

Abstract: We present the theory of site-directed dichroism and its application to the determination of rotational and orientational constraints for oriented polypeptides such as transmembrane helices. Infrared spectroscopy dichroism measurements of single amide I vibrational modes corresponding to ^{13}C-labeled sites within the polypeptide contain information about the helix tilt and rotation angles. This information is readily extracted by analysis of the dichroism of a set of sites along the peptide sequence. Data for just two consecutive sites in the dimeric transmembrane domain of glycophorin A yield the tilt of the helix axis with respect the membrane normal and the rotation of the helix about its axis. By using dichroism data from three consecutive sites, the helix orientation parameters and the orientation of the amide I transition dipole moment, α, can be obtained; the parameters are in close agreement with the solution NMR structure of the glycophorin A peptide dimer and literature values for α. The approach provides orientational information about selectively labeled peptides even under conditions of modest fractional sample order.

1. Introduction

Obtaining high-resolution structures for membrane proteins has proven to be a difficult task, as both NMR and diffraction methods encounter numerous experimental obstacles. Considering the paucity of structural data, any structural insight obtained from other biophysical methods is therefore particularly useful for membrane proteins. Molecular dynamics global search protocols[23] can provide likely structures for membrane proteins that consist of bundles of α-helices, although the method usually requires experimental data to obtain a unique model.[1] While mutagenesis data has sufficed to interpret the molecular dynamics search results, any direct structural measurements would greatly facilitate the predictive power of this method.

Infrared spectroscopy is a particularly useful tool in membrane protein structural analysis that yields information about both the secondary structure and orientation of the protein.[5] Secondary structure is determined by the frequencies of the particular protein's vibrational modes, while the orientation of the protein is related to the observed dichroism. Infrared dichroism is a well-established method for determining order parameters for oriented polymers.[5] The dichroic ratio, $\mathcal{R}$, yields an order parameter, $\mathcal{S}$, that is a measure of both the angle of the molecular director from the z axis and the overall order of the sample.

The order parameter is an average quantity, and as such cannot distinguish between different regions of the polymer because of the limited frequency dispersion of the spectra.

Here FTIR spectroscopy is used to obtain molecular constraints based on site-specific infrared dichroism measurements. The orientation of a single vibrational mode in an α-helix, represented as vector $\bar{P}$ in Figure 1, can be expressed as a function of several parameters: (i) the helix tilt angle β, (ii) the angles α and δ relating the helix axis and the vibrational mode, and (iii) the rotation angle ω of the helix about its axis (see Figure 1). The absorption ratio between parallel and perpendicular polarized light, defined as the dichroic ratio $\mathcal{R}$, for a single vector $\bar{P}$ is related to the projections of the vector $\bar{P}$ on the z axis and on the xy plane together with the integrated absorption coefficients. The orientation of the helix with respect to the axes can therefore be readily extracted given perfect dichroism data, but two practical considerations complicate the process of calculating molecular orientation parameters from experimental dichroic ratios. First, the many vibrational modes in a peptide are located at different rotation angles ω, and therefore have different dichroisms. The frequency overlap of the signals from these many sites means that only the average dichroic ratio of all the differently oriented vibrational modes can be determined, and the information about the helix rotational pitch angle is lost. Second, the sample may be less than perfectly ordered: while a fraction of the helices will be oriented at the angle β, others may be disordered. The absorption by vibrational modes located within disordered peptides will reduce the observed dichroism and affect the calculated helix tilt angle; estimates of the helix tilt angle will then depend on the estimated fractional order of the sample.

† Howard Hughes Medical Institute.

§ Present address: Cambridge University, Department of Biochemistry, 80 Tennis Court Rd., Cambridge, CB2 1GA, UK.

‡ Department of Molecular Biophysics and Biochemistry, Yale University, New Haven, CT 06520.

⊗ Abstract published in *Advance ACS Abstracts,* September 1, 1997.

(1) Adams, P. D.; Arkin, I. T.; Engelman, D. M.; Brunger, A. T. Computational searching and mutagenesis suggest a structure for the pentameric transmembrane domain of phospholamban. *Nat. Struct. Biol.* **1995,** *2* (2), 154−162.

(2) Anderson, T. S.; Hellgeth, J.; Lansbury, P. T. Isotope-edited infrared linear dichroism−determination of amide orientational relationships. *J. Am. Chem. Soc.* **1992,** *31* (51), 6540−6546.

(3) Arkin, I. T.; Rothman, M.; Ludlam, C. F.; Aimoto, S.; Engelman, D. M.; Rothschild, K. J.; Smith, S. O. Structural model of the phospholamban ion channel complex in phospholipid membranes. *J. Mol. Biol.* **1995,** *248* (4), 824−834.
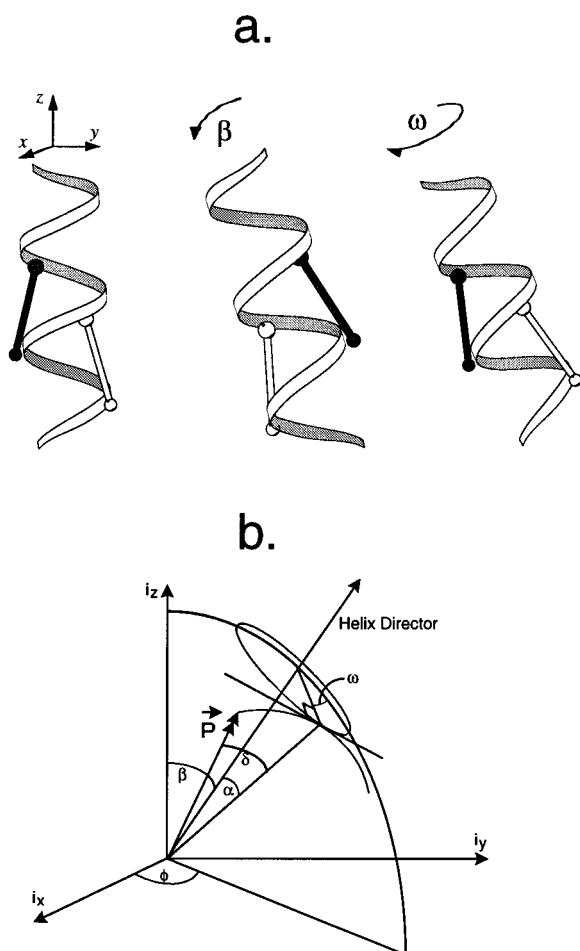
(4) Bradbury, E. M.; Brown, L.; Downie, A. R.; Elliot, A.; Fraser, R. D. B.; Hanby, W. E. The structure of the ω-form of poly-β-benzyl-L-aspartate. *J. Mol. Biol.* **1962,** *5,* 230−247.

(5) Braiman, M. S.; Rothschild, K. J. Fourier transform infrared techniques for probing membrane protein structure. *Annu. Rev. Biophys. Biophys. Chem.* **1988,** *17,* 541−570.

(6) Byler, D. M.; Susi, H. Examination of the secondary structure of proteins by deconvolved FTIR spectra. *Biopolymers* **1986,** *25* (3), 469−487.

(7) Fraser, R. D. B. The interpretation of infrared dichroism in fibrous protein structures. *J. Chem. Phys.* **1996,** *70,* 1511−1515.

(8) Harrick, N. J. *Internal Reflection Spectroscopy*, 1st ed.; Interscience Publishers: New York, 1967.

a.

b.

Figure 1. (a) A schematic diagram of a helix containing two C=O bonds (exaggerated in length for illustrative purposes). The relative orientation of the two bonds, with respect to the z axis, changes upon tilting the helix by the angle β, as well as changing the rotational pitch angle of the helix about its axis by the angle ω. (b) The explicit diagram used in the mathematical derivations of a helix tilted from the z axis by the angle β, containing a vibrating bond, $\vec{P}$, related to the helix director by the angles α and δ. The bond is positioned with a rotational pitch angle ω around the helix director.

Our method overcomes the first of these problems by isotope-label shifting the frequency of a specific vibrational mode so that its dichroism may be directly measured.[2,16,20] The second problem is addressed by using amide I ^{12}C (total) and ^{13}C (site-specific) dichroism data for different sites along the peptide

(9) Hu, W.; Lazo, N. D.; Cross, T. A. Tryptophan dynamics and structural refinement in a lipid bilayer environment: solid state NMR of the gramicidin channel. *Biochemistry* **1995**, *34* (43), 14138−14146.

(10) Kauppinen, J. K.; Moffatt, D. J.; Mantsch, H. H.; Cameron, D. G. Fourier self-deconvolution; a method for resolving intrinsically overlapped bands. *Appl. Spectrosc.* **1982**, *35*, 271−276.

(11) Kraulis, P. J. MOLSCRIPT: A program to produce both detailed and schematic plots of protein structures. *J. Appl. Crystallogr.* **1991**, *24*, 946−950.

(12) Lemmon, M. A.; Flanagan, J. M.; Treutlein, H. R.; Zhang, J.; Engelman, D. M. Sequence specificity in the dimerization of transmembrane α-helices. *Biochemistry* **1992**, *31* (51), 12719−12725.

(13) Lemmon, M. A.; Treutlein H. R.; Adams, P. D.; Brünger, A. T.; Engelman, D. M. A dimerization motif for transmembrane α-helices. *Nat. Struct. Biol.* **1994**, *1* (3), 157−163.

(14) Liu, X. M.; Sonar, S.; Lee, C. P.; Coleman, M.; RajBhandary, U. L.; Rothschild, K. J. Site-directed isotope labeling and FTIR spectroscopy: assignment of tyrosine bands in the bR → M difference spectrum of bacteriorhodopsin. *Biophys. Chem.* **1995**, *56* (1-2), 63−70.

(15) Ludlam, C. F.; Sonar, S.; Lee, C. P.; Coleman, M.; Herzfeld, J.; RajBhandary, U. L.; Rothschild, K. J. Site-directed isotope labeling and ATR-FTIR difference spectroscopy of bacteriorhodopsin: the peptide carbonyl group of Tyr 185 is structurally active during the bR → N transition. *Biochemistry* **1995**, *34* (1), 2−6.

backbone and the direct determination of the fractional order of each of the samples. This analysis is aided by the fact that the relative rotational pitch angles of the labeled sites are known: in α-helices, consecutive sites are related by a 100° rotation.

Comparison of the results with the recently solved solution NMR structure of the glycophorin A transmembrane domain (GpATM[17]) indicates that site-directed dichroism yields quantitative information regarding the tilt and the pitch angles of membrane helices as well as the angle between the transition dipole moment and the helix axis. Furthermore, the multiple measurements decouple the orientational parameters from sample disorder effects (unless complete disorder is present), in contrast to standard order parameter measurements. Using site-directed dichroism in the context of a helix in an oriented polytopic protein could be used to accurately determine the absolute orientation and rotation about the axis of the labeled helix, emphasizing the wide applicability of this method. It should be noted that we have applied this method to a dehydrated bilayer sample which may not be suitable for all reconstituted membrane proteins.

2. Theory

For simplicity we present the theory as it is applied to oriented tilted helices but it should be applicable to any dichroism experiment involving rod-like oriented polymers. Figure 1 presents a schematic model of a helix tilted from the bilayer normal by an angle β. A vibrating bond, denoted by the normalized dimensionless vector $\vec{P}$, is related to the helix director by the angles α and δ, and is distributed around the helix axis as defined by the value of the rotational pitch angle ω. This angle is arbitrarily defined as 0° when the transition dipole moment, the helix director, and the z axis all reside in a single plane (when the angle δ is 0°). As uniaxial symmetry is present in the sample, all results are integrated through every possible ϕ angle.

The dichroic ratio, $\mathcal{R}$, is defined as the absorption ratio between parallel and perpendicular polarized light:

$$\mathcal{R} \equiv \frac{\epsilon_\parallel}{\epsilon_\perp} \tag{1}$$

The absorption of light is equal to the product of the normalized dimensionless electric field components $\mathcal{E}_x$, $\mathcal{E}_y$, and $\mathcal{E}_z$ and the corresponding integrated absorption coefficients $\mathcal{K}_x$, $\mathcal{K}_y$, and $\mathcal{K}_z$. In the case of ATR-FTIR, not taking into account any sample disorder (see below), this expression becomes:[8]

$$\mathcal{R}^{\text{ATR}} = \frac{\mathcal{E}_z^2 \mathcal{K}_z + \mathcal{E}_x^2 \mathcal{K}_x}{\mathcal{E}_y^2 \mathcal{K}_y} \tag{2}$$

The electric field components of the evanescent wave emanating

(16) Ludlam, C. F. C.; Arkin, I. T.; Liu, X.; Rothman, M. S.; Rath, P.; Aimoto, S. O.; Engelman, D. M.; Rothschild, K. J. FTIR spectroscopy and site-directed isotope labelling as a probe of the local secondary structure in the transmembrane domain of phospholamban. *Biophys. J.* **1996**, *70*, 1728−1736.

(17) MacKenzie, K. R.; Prestegard, J. H.; Engelman, D. M. A transmembrane helix dimer: structure and implications. *Science* **1997**, *276*, 131−133.

(18) Patai, S. *The chemistry of the thiol group*, 1st ed.; John Wiley & Sons: London, 1974.

(19) Sonar, S.; Lee, C. P.; Coleman, M.; Patel, N.; Liu, X.; Marti, T.; Khorana, H. G.; RajBhandary, U. L.; Rothschild, K. J. Site-directed isotope labelling and FTIR spectroscopy of bacteriorhodopsin. *Nat. Struct. Biol.* **1994**, *1* (8), 512−517.

(20) Tadesse, L.; Nazarbaghi, R.; Walters, L. Isotopically enhanced infrared spectroscopy: a novel method for examining secondary structure at specific sites in conformationally heterogeneous peptides. *J. Am. Chem. Soc.* **1991**, *113*, 7036−7037.

from the internal reflection element are given by:[8]

$$\mathcal{E}_x = \frac{2\cos\varphi(\sin(\varphi)^2 - n_{21}^2)^{1/2}}{(1 - n_{21}^2)^{1/2}[(1 + n_{21}^2)\sin(\varphi)^2 - n_{21}^2]^{1/2}} = 1.389 \quad (3)$$

$$\mathcal{E}_y = \frac{2\cos\varphi}{(1 - n_{21}^2)^{1/2}} = 1.516 \quad (4)$$

$$\mathcal{E}_z = \frac{2\cos\varphi\sin\varphi}{(1 - n_{21}^2)^{1/2}[(1 + n_{21}^2)\sin(\varphi)^2 - n_{21}^2]^{1/2}} = 1.625 \quad (5)$$

where φ is the angle of incidence between the infrared beam and the internal reflection element (45°), and n_{21} is the ratio between the refractive indices of the sample ($n_2 = 1.43$) and the internal reflection element ($n_1 = 4.0$).[21] These equations are based on the reasonable assumption that the thickness of the deposited film ($>20\ \mu$m) is much larger than the penetration depth (ca. 1 μm) of the evanescent wave.[8] The integrated absorption coefficients $\mathcal{K}_x$, $\mathcal{K}_y$, and $\mathcal{K}_z$ are related to the square of the scalar products of the transition dipole moment, $\vec{P}$, with the appropriate axis $\vec{i}_x$, $\vec{i}_y$, or $\vec{i}_z$ (see Figure 1). Integrating each of the squared scalar products with respect to all ϕ angles (uniaxial symmetry) yields (see Appendix):

$$\mathcal{K}_x(\omega) = \frac{1}{2\pi}\int_0^{2\pi}(\vec{i}_x \cdot \vec{P})^2\,d\phi =$$

$$\frac{1}{2}\cos(\beta)^2\cos(\delta)^2\cos(\omega)^2\sin(\alpha)^2 +$$

$$\cos(\alpha)\cos(\beta)\cos(\delta)^2\cos(\omega)\sin(\alpha)\sin(\beta) +$$

$$\frac{1}{2}\cos(\alpha)^2\cos(\delta)^2\sin(\beta)^2 + \frac{1}{2}\cos(\omega)^2\sin(\delta)^2 +$$

$$\cos(\delta)\cos(\omega)\sin(\alpha)\sin(\delta)\sin(\omega) -$$

$$\cos(\beta)^2\cos(\delta)\cos(\omega)\sin(\alpha)\sin(\delta)\sin(\omega) -$$

$$\cos(\alpha)\cos(\beta)\cos(\delta)\sin(\beta)\sin(\delta)\sin(\omega) +$$

$$\frac{1}{2}\cos(\delta)^2\sin(\alpha)^2\sin(\omega)^2 + \frac{1}{2}\cos(\beta)^2\sin(\delta)^2\sin(\omega)^2 \quad (6)$$

$$\mathcal{K}_y(\omega) = \mathcal{K}_x(\omega) \quad (7)$$

$$\mathcal{K}_z(\omega) = \frac{1}{2\pi}\int_0^{2\pi}(\vec{i}_z \cdot \vec{P})^2\,d\phi = \cos(\alpha)^2\cos(\beta)^2\cos(\delta)^2 -$$

$$2\cos(\alpha)\cos(\beta)\cos(\delta)^2\cos(\omega)\sin(\alpha)\sin(\beta) +$$

$$\cos(\delta)^2\cos(\omega)^2\sin(\alpha)^2\sin(\beta)^2 +$$

$$2\cos(\alpha)\cos(\beta)\cos(\delta)\sin(\beta)\sin(\delta)\sin(\omega) -$$

$$2\cos(\delta)\cos(\omega)\sin(\alpha)\sin(\beta)^2\sin(\delta)\sin(\omega) +$$

$$\sin(\beta)^2\sin(\delta)^2\sin(\omega)^2 \quad (8)$$

Integrating though all possible pitch angles yields the dichroism for an α-helix with vibrational modes rotationally distributed in a random fashion:

$$\mathcal{K}_x(\langle\omega\rangle) = \frac{1}{4\pi^2}\int_0^{2\pi}\int_0^{2\pi}(\vec{i}_x \cdot \vec{P})^2\,d\omega\,d\phi =$$

$$\frac{1}{4}\cos(\beta)^2\cos(\delta)^2\sin(\alpha)^2 + \frac{1}{2}\cos(\alpha)^2\cos(\delta)^2\sin(\beta)^2 +$$

$$\frac{1}{4}\sin(\delta)^2 + \frac{1}{4}\cos(\delta)^2\sin(\alpha)^2 + \frac{1}{4}\cos(\beta)^2\sin(\delta)^2 \quad (9)$$

$$\mathcal{K}_y(\omega) = \mathcal{K}_x(\omega) \quad (10)$$

$$\mathcal{K}_z(\langle\omega\rangle) = \frac{1}{4\pi^2}\int_0^{2\pi}\int_0^{2\pi}(\vec{i}_z \cdot \vec{P})^2\,d\omega\,d\phi =$$

$$\cos(\alpha)^2\cos(\beta)^2\cos(s)^2 + \frac{1}{2}\cos(\delta)^2\sin(\alpha)^2\sin(\beta)^2 +$$

$$\frac{1}{2}\sin(\beta)^2\sin(\delta)^2 \quad (11)$$

So far, the analysis has not taken into account any disorder in the sample. Following Fraser,[7] the fraction of perfectly ordered material about a particular helix tilt is denoted f, and thus $1 - f$ consists of the random fraction. An appropriate correction for the integrated absorption coefficients yields the desired function describing the dichroic ratio:

$$\mathcal{R}^{\text{ATR}}(\omega) = \frac{\mathcal{E}_z^2\left(f\mathcal{K}_z(\omega) + \dfrac{1-f}{3}\right) + \mathcal{E}_x^2\left(f\mathcal{K}_x(\omega) + \dfrac{1-f}{3}\right)}{\mathcal{E}_y^2\left(f\mathcal{K}_y(\omega) + \dfrac{1-f}{3}\right)} \quad (12)$$

whereby the expressions for the integrated absorption coefficients are given in eqs 6–8. For the case of random rotational pitch angles ω, one obtains:

$$\mathcal{R}^{\text{ATR}}(\langle\omega\rangle) =$$

$$\frac{\mathcal{E}_z^2\left(f\mathcal{K}_z(\langle\omega\rangle) + \dfrac{1-f}{3}\right) + \mathcal{E}_x^2\left(f\mathcal{K}_x(\langle\omega\rangle) + \dfrac{1-f}{3}\right)}{\mathcal{E}_y^2\left(f\mathcal{K}_y(\langle\omega\rangle) + \dfrac{1-f}{3}\right)} \quad (13)$$

The equations obtained for the integrated absorption coefficient (eqs 9–11) correspond to those obtained in previous work[7] by setting both angles δ and β to zero. Setting δ to zero reduces the orientational relationship between the transition dipole moment and the helix axis to a single tilt, placing both vectors in the same plane (see Figure 1). It should be noted that for $\beta = 0$, the fractional sample order was shown by Fraser to be the polymer order parameter.[7] In the case of a perfectly ordered sample the polymer director is then coincident with the z axis, which eliminates the dependency on the rotational pitch angle, ω, as seen in eqs 6–8. When the sample is completely disordered (i.e. $f = 0$) then the measured dichroic ratio is simply the ratio between the electric field components, $\mathcal{R}^{\text{ATR}} = (\mathcal{E}_z^2 + \mathcal{E}_x^2)/\mathcal{E}_y^2 = 2.0$.

3. Materials and Methods

1. Glycophorin A Transmembrane Domain Purification and Reconstitution. Peptides were made by standard solid-phase F-moc chemistry. The peptide sequence consisted of amino acids 70–101 of human glycophorin A[22] except for a mutation of I85 to V, shown to be unimportant for dimerization of the protein.[12,13] This amino acid substitution was performed to dramatically reduce the cost of the available isotope labeled amino acid. Three consecutive carbonyl ^{13}C amino acids (Cambridge Isotopes Laboratories, Andover MA) were introduced during synthesis at positions 84, 85, and 86 (numbers correspond to the numbering of human glycophorin A).

After cleaving the peptides from the resin and lyophilization, the peptides were dissolved in TFA (ca. 4 mg/mL) and immediately injected on a C-4 reverse-phase HPLC column (15 × 250 mm Vydac, The Separation Group, Hesperia CA). The column was prequilibrated in 95% water, 2% acetonitrile, and 3% 2-propanol. Elution of the peptides was achieved through a linear gradient, reaching a final solvent composition of 40% acetonitrile and 60% 2-propanol. All HPLC solvents contained 0.1% trifluoroacetic acid. Purified peptides were then lyophilized and subsequently dissolved in a solution of 10% *n-β-*

octylglucoside (Sigma, St. Louis, MO). Peptide reconstitution was achieved by adding to the peptide/detergent solution (final volume 1 mL of 1 mg/mL of peptide) 200 μL of a solution containing 5% n-β-octylglucoside and 25 mg/mL of dimyristoylphosphocholine (Avanti Polar Lipids, Alabaster, AL) followed by exhaustive dialysis into 0.1 mM $Na_2HPO_4 \cdot NaH_2PO_4$ at pH 6.8.

2. FTIR Spectra Collection and Data Processing. Infrared spectra collection and data processing were performed as described previously.[3] Briefly, spectra were collected on a Magna 550 FTIR spectrometer (Nicolet) with an MCT/A detector equipped with a 25 reflections ATR accessory from Grasbey Specac (Kent, UK) and a wire grid polarizer (0.25 μM, Graseby Specac). Four hundred microliters of sample (ca. 1 mg/mL of protein and 5 mg/mL of lipid) were dried onto a Ge trapezoidal internal reflection element (50 $\times$ 2 $\times$ 10 mm). One thousand interferograms were averaged for every sample and processed with 1 point zero filling and Happ-Genzel apodization. Fourier self-deconvolution[10] was applied to the spectra in the amide I region to separate the overlapping ^{12}C and ^{13}C amide I peaks. The enhancement factor used in FSD was 2.0, lower than that previously reported[6] to reduce Fourier ringing.
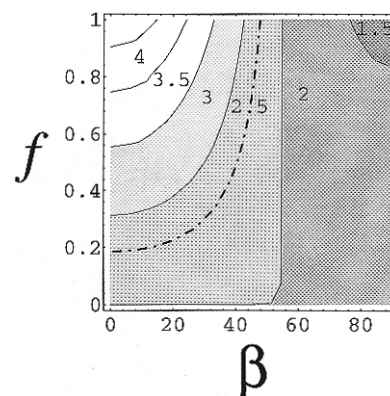
Peak integration was performed for Fourier self-deconvoluted spectra in the regions 1670$-$1645 and 1600$-$1620 cm^{-1} for the helix (^{12}C) and the site-specific label (^{13}C), respectively. In the case of the isotope-shifted amide I peaks, a correction was undertaken for the 1% ^{13}C natural abundance arising from nonlabeled helical segments in the protein. Since the length of the helical segment in the protein is roughly 20$-$25 amino acids, about 20% of the isotope-shifted amide I peak is arising from sources other than the isotope label. The correction is therefore described by the following equation: $\mathcal{R}^{ATR}(\omega)_{corrected} = [5\mathcal{R}^{ATR}(\omega)_{measured} - \mathcal{R}^{ATR}(\langle\omega\rangle)_{measured}]/4$, whereby $\mathcal{R}^{ATR}(\omega)_{measured}$ is the measured dichroic ratio and $\mathcal{R}^{ATR}(\omega)_{corrected}$ is the dichroic ratio used in all subsequent calculations. $\mathcal{R}^{ATR}(\omega)_{measured}$ and $\mathcal{R}^{ATR}(\langle\omega\rangle)_{measured}$ are obtained by dividing the integrated peak areas obtained with parallel and perpendicular polarized light of the site specific label for the ^{13}C amide I band and averaged over the ^{12}C amide I bands of the helix, respectively.

3. Calculations and Error Analysis. All calculations were done with the program Mathematica 2.0 (Wolfram Research, Champaign, IL). Solving the four independent equations was done with Newton's method as implemented in the "FindRoot" function in Mathematica (Wolfram Research, Champaign, IL). The ranges for the calculated tilt and rotational pitch angles were numerically obtained from estimates of the errors of the site-specific dichroism measurements (related to accurate integration of the peak). Upper and lower bounds were obtained by solving the three coupled eqs 6$-$8, adding $\pm$0.1 to each of the observed site-specific dichroisms. These errors reflected the peak integration reproducibility as assessed by repeated measurements. This yielded 27 different bounds, from which the maximum and minimum values were taken in order to derive the error limits on each of the parameters.

4. Results and Discussion

1. Simulation of Dichroic Ratios. a. Random Rotational Pitch Angles, $\mathcal{R}^{ATR}(\langle\omega\rangle)$. Figure 2 depicts the relationship between the tilt angle, β, sample disorder, f, and the measured dichroic ratio for a helix. In this particular case all possible rotational pitch angles are equally probable as described in eq 13. The highest value of the dichroism is obtained at the instance of coincidence with the z axis and no sample disorder. In such a case the dichroic ratio is equal to $\mathcal{R}^{ATR} = 4.4$. The lowest value for the dichroic ratio is obtained at the other limit of the helix tilt where the helix director is in the xy plane. In this case the value for the dichroic ratio is $\mathcal{R}^{ATR} = 1.4$. A sample containing a helix tilted from the z axis by 45° and in which half of the sample is disordered would yield a dichroic ratio of $\mathcal{R}^{ATR} = 2.18$. As stated above, when the sample is completely disordered the dichroic ratio is equal to the ratio between the electric field components and equal to $\mathcal{R}^{ATR} = 2.0$.

In all but the most extreme cases, $\mathcal{R}^{ATR}$ provides a rather broad range of constraints on the helix tilt angle, β. For
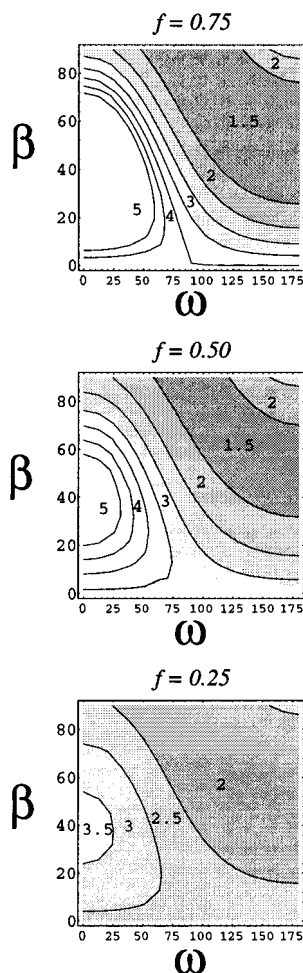

Figure 2. Calculated values for $\mathcal{R}^{ATR}$ as a function of fractional sample order (f) and helix tilt angle (β). The rotational pitch angle, ω, was assumed to be randomly distributed and the calculations were made with eq 13. The tilt angle between the transition dipole moment of the amide I vibrational mode and the helix axis, α, is equal to 39°, but according to definition in Figure 1 is set to 180$-$39°.[24] The angle δ was set to 0°.[24] The maximal value in each contour is depicted. The total plotted range of the dichroic ratio, $\mathcal{R}^{ATR}$, is 1$-$5 in contour levels of 0.5. The dotted line represents a contour line at $\mathcal{R}^{ATR} = 2.3$, the value obtained for the helix dichroic ratio of GpATM.

instance, the value of $\mathcal{R}^{ATR} = 2.5$ might correspond to a sample in which 100% of the sample is tilted at 53° from the bilayer normal. Alternatively, only 19% of the sample may be properly reconstituted, and the tilt angle of those helices is 0°.

b. Unique Rotational Pitch Angles, $\mathcal{R}^{ATR}(\omega)$. The purpose of multiple site-directed dichroism is to extract rotational and orientational information of the relative rotational pitch angles, $\Delta\omega$, if the vibrating modes in a helix are known. As the measured dichroic ratio is a function of three parameters, ω, β, and f (see eq 12), one would need three different measurements using three independent labels to solve for every variable. The two angles relating the transition dipole moment to the helix axis, α and δ, are assumed to be known. However, they too can be extracted with additional labels as shown below.

The influence of the parameters f and β upon the dichroic ratio was simulated with eq 12, leaving each of the two parameters in turn constant (Figures 3 and 4). Inspection of the plots shows that the range of the dichroic ratio obtained from a single vibrational mode with a fixed rotational pitch angle, ω, is much larger than that obtained for a helix in which the rotational pitch angle ω is averaged (Figure 3). When the sum of the tilt angle of the helix and the angle between the transition dipole moment and the helix director $\beta + \alpha = n180°$, $n = 1, 2, ..., n$, and the rotational pitch angle $\omega = 0°$, the transition dipole moment $\vec{P}$ is coincident with the z axis ($\delta = 0°$). In this case the dichroism is infinite ($\mathcal{K}_x = \mathcal{K}_y = 0$). The lowest value for the dichroic ratio is obtained for $f = 1$, when both β and ω are equal to 90°. In this case the dichroic ratio is equal to 0.85 ($\mathcal{K}_z = 0$ and $\mathcal{K}_x = \mathcal{K}_y$). The fact that the site-specific dichroisms can attain values much larger than the helix dichroism is due to the attenuation in the helix dichroism due to multiple averaged rotational pitch angles, ω.

2. Experimental Results. a. ^{13}C Isotope-Shifted Dichroism. Figure 5 shows the raw and Fourier self-deconvoluted ATR-FTIR spectra in the amide I region of three different GpATM transmembrane peptides in oriented lipid bilayers. Each peptide contains a ^{13}C labeled carbonyl in positions 84, 85, or 86, as noted. The dichroic ratios of both the ^{12}C, $\mathcal{R}^{ATR}(\langle\omega\rangle)$, and the isotope-shifted ^{13}C, $\mathcal{R}^{ATR}(\omega)$, amide I peaks are listed in Table 1. Figure 6 depict spectra obtained in a identical manner for a peptide containing no ^{13}C labels (note the lack of isotope shifted peak at 1614 cm^{-1}).

Site-Directed Dichroism

J. Am. Chem. Soc., Vol. 119, No. 38, 1997 8977

Figure 3. Calculated values for $\mathcal{R}^{ATR}$ as a function of helix tilt angle (β) and rotational pitch angle (ω). Equation 12 was used to calculate values of $\mathcal{R}^{ATR}$ for three values of the fractional sample disorder, f. The values for the angles relating the transition dipole moment and the helix axis, α and δ, are set to 141° and 0°.[24] The maximal value in each contour is depicted. The total plotted range of the dichroic ratio, $\mathcal{R}^{ATR}$, is 1−5 in contour levels of 0.5.
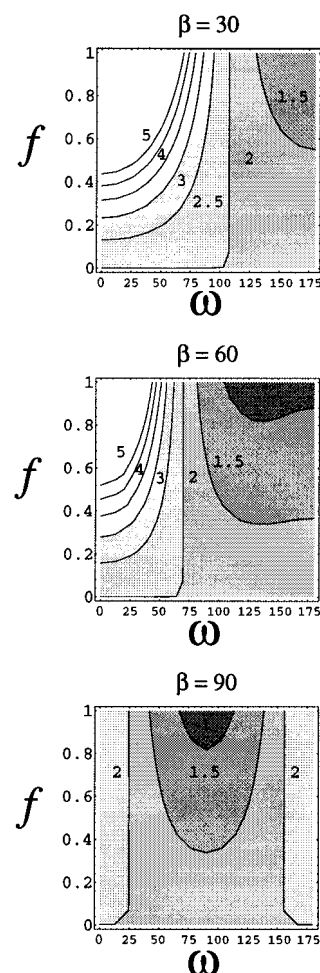
b. Data Analysis. The factors that influence the measured dichroic ratios, following eqs 6−8 (Figure 1) are the following: (1) α and δ are angles relating the orientation of the transition dipole moment with respect to the helix director; (2) β is the tilt angle of the helix director; (3) f is the overall sample ordered fraction; and (4) ω is the rotational pitch angle of the sample, which influences only the site-specific dichroism. It is assumed that α, δ, and β are identical in the three different GpATM mutants. Furthermore, it is also assumed that due to symmetry each of the polypeptide chains is identical and therefore has the same α, δ, and β orientational angles. The angles α and δ have been measured for oriented fibers of poly-(γ-benzyl L-glutamate) and shown to be 141° and 0°, respectively.[24] It is also assumed that the rotational pitch angle

(21) Tamm, L. K.; Tatulian, S. A. Orientation of functional and nonfunctional PTS permease signal sequences in lipid bilayers. A polarized attenuated total reflection infrared study. *Biochemistry* **1993**, *32* (30), 7720−7726.

(22) Tomita, M.; Marchesi, V. T. Amino-acid sequence and oligosaccharide attachment sites of human erythrocyte glycophorin. *Proc. Natl. Acad. Sci. U.S.A.* **1975**, *72* (8), 2964−2968.

(23) Treutlein, H. R.; Lemmon, M. A.; Engelman, D. M.; Brunger, A. T. The glycophorin A transmembrane domain dimer: sequence-specific propensity for a right-handed supercoil of helices. *Biochemistry* **1992**, *31* (51), 12726−12732.

(24) Tsuboi, M. Infrared dichorism and molecular conformation of α-form poly-γ-benzyl-L-glutamate. *J. Polym. Sci.* **1962**, *59*, 139−153.
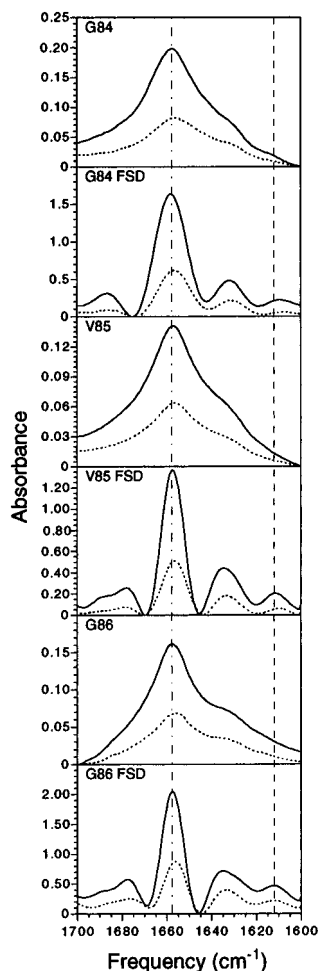
Figure 4. Calculated values for $\mathcal{R}^{ATR}$ as a function of fractional sample disorder (f) and helix rotational pitch angle (ω). Equation 12 was used to calculate values of $\mathcal{R}^{ATR}$ for three values of the helix tilt angle, β. The values for the angles relating the transition dipole moment and the helix axis, α and δ, are set to 141° and 0°.[24] The maximal value in each contour is depicted. The total plotted range of the dichroic ratio, $\mathcal{R}^{ATR}$, is 1−5 in contour levels of 0.5.

of the helix is constant and the difference in ω between the three labeled sites is simply the α-helix increment of 100°. Since the observed helix dichroic ratios of the three peptides are within experimental error, one can safely conclude that the fraction of perfectly ordered sample at a defined tilt angle, f, is the same in all three peptides (see eq 13).

The data obtained consist of four measurements for the GpATM peptides: the average helix dichroic ratio and the site-specific dichroic ratios for the three labels. Each of these measurements yields an independent constraint that can be used to solve for the three unknowns: β, f, and ω. Equation 13 is used for the helix dichroic ratio, while eq 12 is used for the site-specific dichroism. Since the rotational pitch difference between the two different site-specific labels is 100° (assuming no gross distortions in the helix), one can set the angles of G84, V85, and G86 to be ω, $\omega + 100°$, and $\omega + 200°$, respectively. Because the data yield four independent equations (one for the helix and three for each of the different ^{13}C labels), it is possible to solve for the tilt angle between the transition dipole moment and the helix axis, α. It is therefore possible to measure α in an independent manner within the specific sample as opposed to using values drived from a model compound.

The resulting tilt angle of the helix, β, is 26° (+7°, −6°), while the fraction of perfectly ordered sample, f, is 0.26 (+0.04,

Figure 5. ATR-FTIR spectra of GpATM peptides in lipid bilayers. Spectra obtained with parallel and perpendicular polarized light are depicted with solid and dotted lines, respectively. Top, middle and bottom two panels present spectra of GpATM with carbonyl ^{13}C at positions 84, 85, and 86, respectively. "FSD" indicates Fourier self-deconvoluted spectra using a band width at half height of 13 cm^{-1} and a resolution enhancement factor of 2.0.[6] The two dotted lines as 1657 and 1613 cm^{-1} represent the ^{12}C and ^{13}C amide I bands, respectively. The peaks at 1633 and 1675 may correspond to β-sheet components in the extramembranous segment of the peptide.[6]

Table 1. Helix and Site-Specific Dichroism Data for Glycophorin A Transmembrane Peptides with [13]C Labeled Carbonyls at the Sequence Positions Indicated[a]
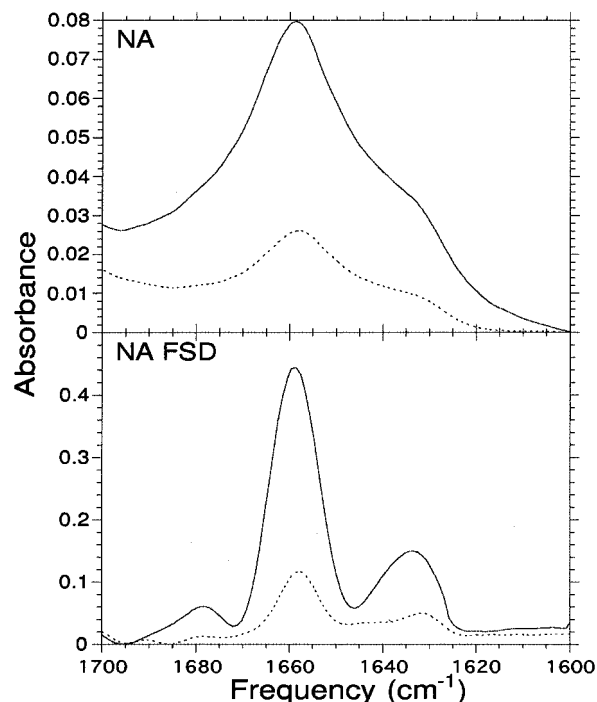
peptide	helix dichroism	site-specific dichroism[b]
carbonyl [13]C G84	$R^{ATR}(\langle\omega\rangle) = 2.25 \pm 0.1$	$R^{ATR}(\omega) = 2.9 \pm 0.1$
carbonyl [13]C V85	$R^{ATR}(\langle\omega\rangle) = 2.3 \pm 0.1$	$R^{ATR}(\omega) = 2.6 \pm 0.1$
carbonyl [13]C G86	$R^{ATR}(\langle\omega\rangle) = 2.25 \pm 0.1$	$R^{ATR}(\omega) = 1.8 \pm 0.1$

[a] Helix dichroism is calculated for absorption between 1645 and 1665 cm^{-1}, corresponding to the "natural abundance, [12]C" amide I mode. Site-specific dichroism is calculated for absorption between 1605 and 1625 cm^{-1}, corresponding to the isotope-shifted, ^{13}C amide I mode.[20] [b] The site-specific dichroism is corrected for natural abundance of the ^{13}C of the amide I mode arising from the "unlabeled" segment of the protein, as described in Materials and Methods.

-0.03). The rotational pitch angle for residue G84, ω, is 323° ($+10°$, $-12°$) (see Table 2). The rotational pitch angle, ω, for residues V85 and G86 is simply 323° + 100° = 63° ($+10°$, $-12°$) and 323° + 200° = 163° ($+10°$, $-12°$), respectively, due to the helix increment.

In this particular case it was possible to measure the helix dichroic ratio since the isolated GpATM peptide, although dimeric, contains only a single helix species. In the more

Figure 6. Same as Figure 5 but for a GpATM containing no ^{13}C labels.

Table 2. Comparison between Independent Data and the Results Obtained by Site-Directed Dichroism, for GpATM, Carbonyl ^{13}C at G84[a]
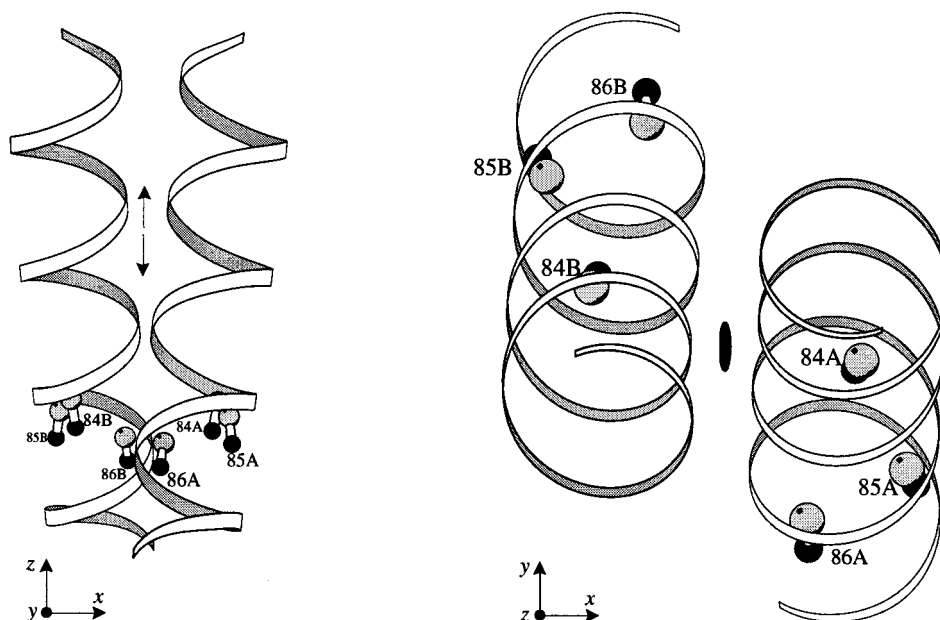
parameter	independent data	site-directed dichroism
helix tilt	$\beta = 20°$	$\beta = 26°$ ($+7°$, $-6°$)
rotational pitch	$\omega = 341°$	$\omega = 323°$ ($+10°$, $-12°$)
transition dipole tilt	$\alpha = 39°$	$\alpha = 41°$ ($+5°$, $-2°$)

[a] Both β and ω were independently obtained from the solution NMR structure. The rotational pitch angle, ω, is with respect to amino acid G84. The transition dipole moment α cannot be determined by the NMR structure but is compared to values in the literature.[4,24] The errors associated with the calculated results are computed as described in the text.

general case of a transmembrane helix in a polytopic protein, this kind of measurement would not be possible. Thus, one would only obtain three independent equations representing each of the site-specific dichroism measurements. In this case it should be possible to solve for the helix tilt, β, pitch angle, ω, as well as the fractional sample order, f, assuming a fixed helix. This was demonstrated in the glycophorin peptide when the angle between the transition dipole moment and the helix axis, α, was set to 41°. The results obtained were identical with those described above. These results demonstrate that for a large polytopic membrane protein, it should be possible to determine the orientation of a particular helix. Taking these measurements for several helices within the protein should therefore greatly restrict the number of possible low-resolution models for the particular protein.

It is instructive to compare the results obtained from the analysis developed in this method to those obtained from conventional dichroism analysis. As stated in the Theory section such analysis is performed on the dichroic ratio obtained from the helix and yields an order parameter S. This order parameter is equivalent to the fractional sample order f when the tilt angle of the helix β is equal to zero.

As seen in Figure 2, the conventional analysis of the helix dichroism data yields a relationship between the helix tilt angle and the fractional sample order as a function of the dichroic ratio. The data restrict the maximal tilt angle of the helix from

Figure 7. Ribbon diagram of the transmembrane segment of human GpATM based on the structure determined for the protein by multi-dimensional NMR in detergent micelles.[17] In the right-hand structure the dyad/symmetry axis of the system is pointed toward the reader and is coincident with the z axis depicted in the lower left-hand corner of the figure. The C=O bonds of the protein at positions G84, V85, and G86 are indicated to facilitate visualization of the extent of orientation with the indicated z axis. The figure was generated with Molscript.[11]

the bilayer normal to 47°. In the case where the tilt angle, β, is 47°, the fractional sample order, f, is equal to 1. However, a tilt angle β equal to zero would also be consistent with these data when setting the value for the fractional sample order equal to the order parameter, $f = S = 0.197$. Without an experimental measure of the sample fractional order f, this analysis cannot accurately define the helix orientation.

c. Comparison with Independent Data. The comparison between the results obtained by site-directed dichroism is in close agreement to data obtained by independent studies (see Table 2). As is qualitatively seen in Figure 7, the extent of parallel orientation of the three different ^{13}C=O bonds at positions G84, V85, and G86 corresponds to their site-specific dichroism. The most parallel bond (G84) exhibits a higher dichroic ratio as expected, while the least dichroic bond at G86 exhibits the highest degree of tilt. Quantitatively, the helix tilt calculated in this study to be 26° agrees very well with the value measured for the solution NMR structure of 20°.

The rotational pitch angle of the two residues measured in this study is 323°, 63°, and 163° for G84, V85, and G86, respectively. Note that an angle of 0° would correspond to a residue positioned at the bottom face of the helix in the direction of the tilt, as is the case for G84. G86 on the other hand is seen on the top of the tilted helix and therefore the calculated pitch angle of 163° agrees well with the model as shown in Figure 7.

The value obtained for the angle between the transition dipole moment and the helix axis is again in close agreement with measured values. The value obtained, $\alpha = 41°$, is similar to values reported in the literature: 39−40°.[4,24]

5. Conclusions

The new method presented here, site-directed dichroism, enables the determination of the helix tilt angle, β, and pitch angle, ω, from two selectively labeled oriented samples. Our results for glycophorin A agree with the solution NMR structure of the peptide dimer despite the fact that the dichroism experiments were carried out on samples having only a small fraction (25%) of well-ordered peptide. Our results demonstrate

that this method provides significant advantages over conventional FTIR dichroism experiments, and opens the possibility of determining helix tilt and pitch angles in helices of polytopic membrane proteins. These orientational constraints could have great value in distinguishing between models for protein structures based on modeling, mutagenesis, or sequence alignment methods.

Rotational and orientational constraints for membrane proteins can also be obtained by solid-state NMR spectroscopy of labeled, oriented samples: the orientation of a dipolar or quadrupolar chemical shift tensor is measured, and the molecular coordinates inferred. The fact that lipid membranes readily form oriented multilayers has enabled the application of this method to many systems, especially gramicidin A, whose structure in oriented bilayers has been determined from orientational constraints alone.[9] Compared with site-directed dichroism, this method has the disadvantage of requiring large samples (several milligrams of labeled peptide), limiting it to synthetic peptides and resulting in very high protein-to-lipid ratios. Solid-state NMR methods do have the advantage of potentially resolving the contributions of multiple labels in a single sample. Useful labeling schemes for NMR will not always coincide with useful labels for site-directed dichroism, but the similarity of the type of information obtained from the two methods suggests that they might be combined productively.

The choice of site-specific labels is clearly limited. Use of ^{13}C requires either synthetic peptides or a cell-free expression system.[14,15,19] In a protein larger than 100 amino acids, however, the ^{13}C signal would be dominated by the natural abundance of ^{13}C. An alternative isotopic label would be deuterium substituted at the α position of a given amino acid. This results in a large vibrational shift and virtually no natural abundance. ^{15}N, while an excellent nucleus for oriented solid-state NMR experiments, would be technically difficult to exploit in site-directed dichroism as the vibrational mode that is shifted the farthest (N−H) is obscured by the H_2O absorption.

An additional target should be the S−H group of cysteine residues, which exhibit a weak but resolved vibrational mode at 2500−2600 cm^{-1}.[18] In a helix, these side chains would most

likely form hydrogen bonds to the $(i - 4)$ carbonyl oxygen (detected by the shift of the S−H vibration), providing a transition dipole of known orientation that could be exploited in these studies. Utilizing sulfhydryl vibrational modes would expand the applicability of this method to nearly any membrane protein that can be manipulated genetically but that are otherwise not tractable in solid-state NMR methods. A series of cysteine substitutions followed by measurements of dichroism at consecutive positions would produce the absolute tilt and pitch angles for each helix.

Appendix

Here we derive the equations for the integrated absoption coefficients, $\mathcal{K}_x$, $\mathcal{K}_y$, and $\mathcal{K}_z$ (eqs 6−8). These coefficients are calculated by deriving the Cartesian coordinates of the vibrational transition dipole moment, $\vec{P}$, by a set of rotation matrices. The coordinates are then squared and subsequently averaged over all values of the angle ϕ to satisfy uniaxial symmetry. The definitions for the three axial rotation matrices are

$$R_x(\theta) = \begin{pmatrix} 1 & 0 & 0 \\ 0 & \cos\theta & -\sin\theta \\ 0 & \sin\theta & \cos\theta \end{pmatrix}$$

$$R_y(\theta) = \begin{pmatrix} \cos\theta & 0 & \sin\theta \\ 0 & 1 & 0 \\ -\sin\theta & 0 & \cos\theta \end{pmatrix}$$

$$R_z(\theta) = \begin{pmatrix} \cos\theta & -\sin\theta & 0 \\ \sin\theta & \cos\theta & 0 \\ 0 & 0 & 1 \end{pmatrix} \quad \text{(A.1)}$$

The Cartesian coordinates of the vibrational transition dipole moment, $\vec{P}$, are then given by the following matrices:

$$R_z(\phi)\cdot R_x(-\beta)\cdot R_z(\omega)\cdot R_x(-\alpha)\cdot R_y(\delta)\cdot \begin{pmatrix} 0 \\ 0 \\ 1 \end{pmatrix} \quad \text{(A.2)}$$

and explicitly

$$\vec{i}_x\cdot\vec{P} = -[\cos(\beta)\cos(\delta)\cos(\omega)\cos(\phi)\sin(\alpha)] - \\ \cos(\alpha)\cos(\delta)\cos(\phi)\sin(\beta) + \\ \cos(\beta)\cos(\phi)\sin(\delta)\sin(\omega)\cos(\omega)\sin(\delta)\sin(\phi) + \\ \cos(\delta)\sin(\alpha)\sin(\omega)\sin(\phi) \quad \text{(A.3)}$$

$$\vec{i}_y\cdot\vec{P} = \cos(\omega)\cos(\phi)\sin(\delta) + \\ \cos(\delta)\cos(\phi)\sin(\alpha)\sin(\omega) + \\ \cos(\beta)\cos(\delta)\cos(\omega)\sin(\alpha)\sin(\phi) + \\ \cos(\alpha)\cos(\delta)\sin(\beta)\sin(\phi) - \\ \cos(\beta)\sin(\delta)\sin(\omega)\sin(\phi) \quad \text{(A.4)}$$

$$\vec{i}_z\cdot\vec{P} = \cos(\alpha)\cos(\beta)\cos(\delta) - \\ \cos(\delta)\cos(\omega)\sin(\alpha)\sin(\beta) + \sin(\beta)\sin(\delta)\sin(\omega) \quad \text{(A.5)}$$

We now square the coordinates to obtain the absorption intensities:

$$(\vec{i}_x\cdot\vec{P})^2 = \cos(\beta)^2\cos(\delta)^2\cos(\omega)^2\cos(\phi)^2\sin(\alpha)^2 + \\ 2\cos(\alpha)\cos(\beta)\cos(\delta)^2\cos(\omega)\cos(\phi)^2\sin(\alpha)\sin(\beta) + \\ \cos(\alpha)^2\cos(\delta)^2\cos(\phi)^2\sin(\beta)^2 - \\ 2\cos(\beta)^2\cos(\delta)\cos(\omega)\cos(\phi)^2\sin(\alpha)\sin(\delta)\sin(\omega) - \\ 2\cos(\alpha)\cos(\beta)\cos(\delta)\cos(\phi)^2\sin(\beta)\sin(\delta)\sin(\omega) + \\ \cos(\beta)^2\cos(\phi)^2\sin(\delta)^2\sin(\omega)^2 - \\ 2\cos(\beta)\cos(\delta)\cos(\omega)^2\cos(\phi)\sin(\alpha)\sin(\delta)\sin(\phi) - \\ 2\cos(\alpha)\cos(\delta)\cos(\omega)\cos(\phi)\sin(\beta)\sin(\delta)\sin(\phi) - \\ 2\cos(\beta)\cos(\delta)^2\cos(\omega)\cos(\phi)\sin(\alpha)^2\sin(\omega)\sin(\phi) - \\ 2\cos(\alpha)\cos(\delta)^2\cos(\phi)\sin(\alpha)\sin(\beta)\sin(\omega)\sin(\phi) + \\ 2\cos(\beta)\cos(\omega)\cos(\phi)\sin(\delta)^2\sin(\omega)\sin(\phi) + \\ 2\cos(\beta)\cos(\delta)\cos(\phi)\sin(\alpha)\sin(\delta)\sin(\omega)^2\sin(\phi) + \\ \cos(\omega)^2\sin(\delta)^2\sin(\phi)^2 + \cos(\delta)^2\sin(\alpha)^2\sin(\omega)^2\sin(\phi)^2 + \\ 2\cos(\delta)\cos(\omega)\sin(\alpha)\sin(\delta)\sin(\omega)\sin(\phi)^2 \quad \text{(A.6)}$$

$$(\vec{i}_y\cdot\vec{P})^2 = \cos(\omega)^2\cos(\phi)^2\sin(\delta)^2 + \\ 2\cos(\delta)\cos(\omega)\cos(\phi)^2\sin(\alpha)\sin(\delta)\sin(\omega) + \\ \cos(\delta)^2\cos(\phi)^2\sin(\alpha)^2\sin(\omega)^2 + \\ 2\cos(\beta)\cos(\delta)\cos(\omega)^2\cos(\phi)\sin(\alpha)\sin(\delta)\sin(\phi) + \\ 2\cos(\alpha)\cos(\delta)\cos(\omega)\cos(\phi)\sin(\beta)\sin(\delta)\sin(\phi) + \\ 2\cos(\beta)\cos(\delta)^2\cos(\omega)\cos(\phi)\sin(\alpha)^2\sin(\omega)\sin(\phi) + \\ 2\cos(\alpha)\cos(\delta)^2\cos(\phi)\sin(\alpha)\sin(\beta)\sin(\omega)\sin(\phi) - \\ 2\cos(\beta)\cos(\omega)\cos(\phi)\sin(\delta)^2\sin(\omega)\sin(\phi) - \\ 2\cos(\beta)\cos(\delta)\cos(\phi)\sin(\alpha)\sin(\delta)\sin(\omega)^2\sin(\phi) + \\ \cos(\beta)^2\cos(\delta)^2\cos(\omega)^2\sin(\alpha)^2\sin(\phi)^2 + \\ 2\cos(\alpha)\cos(\beta)\cos(\delta)^2\cos(\omega)\sin(\alpha)\sin(\beta)\sin(\phi)^2 + \\ \cos(\alpha)^2\cos(\delta)^2\sin(\beta)^2\sin(\phi)^2 - \\ 2\cos(\beta)^2\cos(\delta)\cos(\omega)\sin(\alpha)\sin(\delta)\sin(\omega)\sin(\phi)^2 - \\ 2\cos(\alpha)\cos(\beta)\cos(\delta)\sin(\beta)\sin(\delta)\sin(\omega)\sin(\phi)^2 + \\ \cos(\beta)^2\sin(\delta)^2\sin(\omega)^2\sin(\phi)^2 \quad \text{(A.7)}$$

$$(\vec{i}_z\cdot\vec{P})^2 = \cos(\alpha)^2\cos(\beta)^2\cos(\delta)^2 - \\ 2\cos(\alpha)\cos(\beta)\cos(\delta)^2\cos(\omega)\sin(\alpha)\sin(\beta) + \\ \cos(\delta)^2\cos(\omega)^2\sin(\alpha)^2\sin(\beta)^2 + \\ 2\cos(\alpha)\cos(\beta)\cos(\delta)\sin(\beta)\sin(\delta)\sin(\omega) - \\ 2\cos(\delta)\cos(\omega)\sin(\alpha)\sin(\beta)^2\sin(\delta)\sin(\omega) + \\ \sin(\beta)^2\sin(\delta)^2\sin(\omega)^2 \quad \text{(A.8)}$$

Integrating through all possible ϕ angles due to uniaxial symmetry by using the following relationships

$$\langle\cos(\phi)^2\rangle = \langle\cos(\phi)^2\rangle = {}^1/_2$$

$$\langle\cos(\phi)\sin(\phi)\rangle = \langle\cos(\phi)\rangle = \langle\sin(\phi)\rangle = 0 \quad \text{(A.9)}$$

yields the desired equations for the integrated absorption coefficients (eqs 6−8).